Chinese Chemical Letters 36 (2025) 110427

Contents lists available at ScienceDirect

Chinese Chemical Letters

journal homepage: www.elsevier.com/locate/cclet

Chalcone-derived oxime esters with efficient photoinitiation properties under LED irradiation

Qian Wu, Mengda Xu, Tianjiao Ma, Shuzhen Yan, Jin Li*, Xuesong Jiang*

School of Chemistry& Chemical Engineering, Frontiers Science Center for Transformative Molecules, State Key Laboratory for Metal Matrix Composite Materials, Shanghai Jiao Tong University, Shanghai 200240, China

ARTICLE INFO

Article history:
Received 21 June 2024
Revised 2 September 2024
Accepted 6 September 2024
Available online 13 September 2024

Keywords:
Photopolymerization
Photoinitiator
Chalcone
Oxime ester
Free radical polymerization

ABSTRACT

As one of the most essential components in photocuring system, photoinitiators (PIs) exert a crucial influence on the properties of the cured product. However, commercially available PIs encounter challenges in simultaneously achieving efficient photoinitiation performance and excellent light absorption properties, significantly limiting their applications in various fields. Here, two bis-chalcones and four corresponding oxime esters (OXEs) were designed and synthesized as highly efficient PIs. Featuring a structure comprising bis-chalcone and two diphenyl sulfides, the conjugated systems in these compounds enhance their light-absorption properties in near-ultraviolet and visible region, effectively. Both the frontier molecular orbital simulations and excited state calculations suggest the contribution of sulfur atoms to electron delocalization and the formation of conjugated structure. Due to the high reactivity of the N–O bond in OXE moiety, the four OXEs exhibit exceptional free radical photoinitiating ability in commercial acrylic monomers/oligomers with LED@365 nm as light source. Notably, one of them demonstrates superior performance in the photoinitiation of multifunctional crosslinker, achieving more than 70% conversion within 3 s, coupled with outstanding absorption at 365 nm. These chalcone-based OXEs are considered to exert significant potential in the realm of free radical photocuring.

Possessing the "5E" (Efficient, Energy Saving, Environmentally Friendly, Economical and Enabling) characteristic, photopolymerization has been extensively utilized across various critical fields, such as 3D printing, photoresists and coatings [1-14]. Photoinitiators (PIs), as crucial components in photocuring formulations, determine the rate of photopolymerization, thereby exerting an essential influence on the properties of the resultant products. However, commercially available PIs confront significant challenges as conventional light sources are gradually being replaced by light-emitting diode (LED) [15]. Specifically, LED has narrower wavelength range and lower power compared to conventional mercury lamp. For this reason, massive traditional commercial PIs would be eliminated for the insufficient light-absorption properties. To address this issue, researchers have focused on enhancing the light-absorption properties of PIs [16-21]. For example, Wang *et al.* designed a series of dyes with double benzylidene ketone structure, which exhibits notable light-absorption within the visible light region [17]. However, due to the intrinsic diffusion limitations of Type II PIs and co-initiators, their photoinitiating rates are unsatisfactory, constraining their practical applications [3,22-24]. Therefore, there is a pressing need to develop novel PIs that combine exceptional light-absorption properties with outstanding photoinitiating abilities.

Chemical structure invariably exerts a significant influence on compound performance. Therefore, it is prudent to balance the photoinitiating abilities and light-absorption properties by introducing chemical moieties properly for PIs' molecule design. Chalcones, the cornerstone of numerous biologically intriguing compounds sourced from nature, have garnered substantial research attention over decades [16,25]. Due to their brilliant light-absorption properties and photosensitivity, chalcones have been used in photocuring either as Type II PIs or photosensitizers [26-33]. Recently, Chen *et al.* have successfully introduced triphenylamine into four chalcone structures as one-component Type II PIs, improving the absorption in visible-light region obviously [26,27]. Meanwhile, chalcone has favorable energy interaction with iodonium salt (Iod) [28], leading to the development of three-component photoinitiating systems comprising chalcone, Iod, and co-initiator [29-31,34]. These systems demonstrate impressive light-absorption properties and photoinitiating abilities in both radical and cationic photopolymerizations. However, the extensive

* Corresponding authors.
E-mail addresses: 13travelling@sjtu.edu.cn (J. Li), ponygle@sjtu.edu.cn (X. Jiang).

https://doi.org/10.1016/j.cclet.2024.110427
1001-8417/

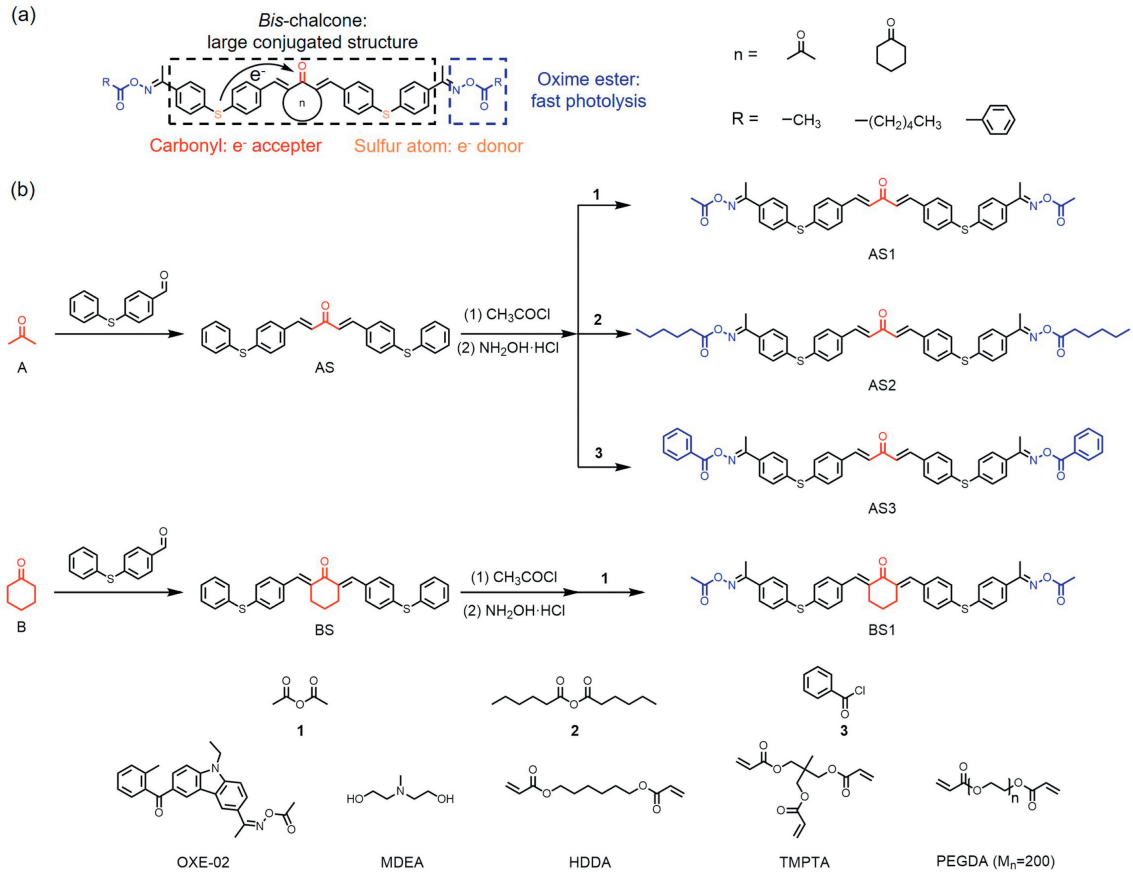

Fig. 1. (a) The construction strategy of chalcone-based OXEs. (b) Synthesis routes of AS1, AS2, AS3 and BS1.

usage of iodonium salt has greatly increased the cost. In addition, researchers have improved the photoinitiating performance of chalcones by incorporating the oxime ester (OXE) moiety [35-37], which triggers the formation of highly active free radicals through the photolysis of the N–O bond [22,38-41]. Tang *et al.* introduced the OXE moiety into cyclopentanone-based chalcone successfully, resulting in PIs with outstanding light-absorption property and photobleaching ability [35]. Nevertheless, the ring structure of cyclopentanone exhibited negative influences on the formation of conjugated system and electron transfer, thereby diminishing the photoinitiating rate [42]. Hence, it is imperative to fully exploit the advantages of both the chalcone moiety and the OXE moiety through meticulous molecular design, achieving high photoinitiating performance and excellent light-absorption properties simultaneously.

In this study, chalcone, diphenyl sulfide and OXE were unprecedentedly combined together, giving four chalcone-based OXEs (Fig. 1a). These OXEs exhibited outstanding light-absorption properties in the near ultraviolet and visible light region, which was attributed to the large conjugated system comprising chalcone and two diphenyl sulfides. Additionally, electron delocalization and electron transfer over whole molecule of four OXEs were confirmed by energy level transition calculations and frontier molecular orbital simulations, validating the efficacy of the structure design strategy. Moreover, real-time Fouriertransform infrared spectroscopy (RT-FTIR) and photorheological experiments demonstrated the excellent photoinitiating abilities of these OXEs in acrylic monomers/oligomers under near-ultraviolet LED, highlighting the significant contribution of the OXE moiety. The construction strategy proposed here effectively maximizes the advantages offered by three moieties (chalcone, diphenyl sulfide and OXE), achieving outstanding photoinitiating abilities and excellent light-absorption properties simultaneously.

The chalcone structure exhibits brilliant photobleaching ability and notable light-absorption in visible light region, and the moiety connected to the chalcone determines its characterizations. Hence, diphenyl sulfide was selected to play this role in consider of its impressive conjugation effect [40,43]. Specifically, a bis-chalcone (AS) was synthesized *via* an Aldol condensation reaction. Featuring a bis-chalcone moiety and two benzene sulfides, AS boasts a large conjugated system symmetrically delocalized throughout. Furthermore, the lone electron pairs of sulfur atoms in diphenyl sulfide provide strong electron push-pull effect *via* p-π conjugation, significantly enhancing the conjugated system and electron transfer properties. The conjugated structure and electron transfer were identified by theoretical calculations. In addition, another bis-chalcone (BS) was also synthesized to explore the influence of ring structure. Subsequently, OXE moiety was introduced into two bis-chalcones to achieve enhanced photoinitiating performance. Since the photoinitiating abilities of OXEs are significantly influenced by the substituents attached to ester group [22], three distinct substituents were carefully selected to impart diverse characteristics into OXEs. The structures and synthesis route of two bis-chalcones (AS and BS) and four OXEs (AS1, AS2, AS3 and BS1) derived from them were outlined in Fig. 1b.

Taking AS1 as an example, the synthesis process of OXEs was discussed in detail. Firstly, bis-chalcone AS was synthesized through an Aldol condensation reaction with acetone and two 4-(phenylthio)benzaldehydes. As illustrated by the ^{1}H NMR spectrum (Fig. 2a), the resonance signals assigned to the vinyl protons (H_1 and H_2) appeared, indicating the successful synthesis of AS. Subsequently, the carbonyl group was introduced to form 1-AS through

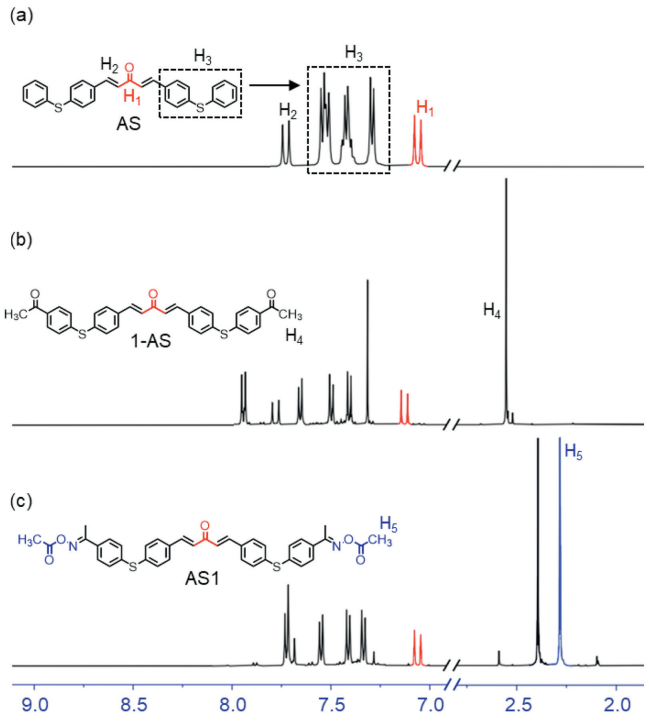

Fig. 2. ^{1}H NMR spectra of (a) AS, (b) 1-AS and (c) AS1 (500 MHz, $CDCl_3$, 298 K).

a Friedel-Crafts reaction, which was confirmed by the resonance signal of methyl protons (H_4) in Fig. 2b. The OXE moiety was introduced through two consecutive steps, including a reducing reaction with hydroxylamine hydrochloride and an esterification reaction with acetic anhydride. A resonance signal assigned to the methyl protons (H_5) on the ester group was observed (Fig. 2c), demonstrating the successful synthesis of AS1. Detailed synthesis methods for other compounds were depicted, and the structures of PIs were confirmed using ^{1}H NMR, ^{13}C NMR and HRMS (Scheme S1 and Figs. S2-S17 in Supporting information).

In order to check the light-absorption properties of chalcones and OXEs, ultraviolet-visible (UV-vis) absorption spectra and fluorescence emission spectra of six compounds were conducted (Fig. 3 and Fig. S18 in Supporting information). High similarities between chalcones and their derived OXEs have been observed according to the results, indicating the significant influence of the chalcone moiety on OXEs. As shown in Fig. 3a, it is evident that two bis-chalcones exhibited strong light absorption properties with absorption peaks around 360 nm. This remarkable absorption property of AS and BS stems from their conjugated system, which comprises the chalcone structure and the connected benzene sulfides. Meanwhile, four OXEs, exhibiting strong absorption at 365 nm, inherited the outstanding light-absorption properties observed in chalcones (Fig. 3b). All of the four OXEs showed superior absorption than that of the commercial OXE-02. It is noteworthy that the cyclic structure in BS1 showed a negative influence on the absorption property, evident by the blue shift of the absorption peak and the decline in absorption coefficient (Table S1 in Supporting information). Additionally, as shown in Fig. S18a, chalcones and OXEs displayed analogous low fluorescence emission intensity except AS3, implying a propensity for non-radiative deexcitation processes [44], such as the generation of free radicals. Interestingly, unlike other compounds, AS3 showed a relatively strong fluorescence emission intensity, which could be attributed to the benzene in the OXE moiety. Detailed absorption data for chalcones and OXEs were provided in Table S1.

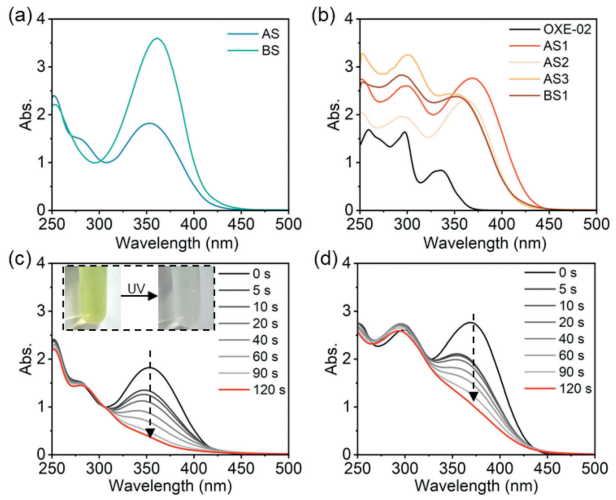

Fig. 3. UV–vis absorption spectra of (a) bis-chalcones and (b) OXEs. Steady-state photolysis curve of (c) AS and (d) AS1. All tests were conducted in ethyl acetate with PI's concentration of 1×10^{-4} mol/L under 365 nm LED, and the light intensity is 100 mW/cm^2.

Interestingly, AS1, AS2, and AS3, all derived from AS, exhibited distinct absorption peaks and absorption coefficients, which could be attributed to the influence of dihedral angles. As illustrated in Fig. S19 (Supporting information), the dihedral angle between the chalcone plane and the connected benzene plane in AS and its derivatives were outlined. Their geometric structures were optimized *via* CAM-B3LYP/6–31G level calculations. For AS1, AS2 and AS3, the size of dihedral angles ($D_{AS1} < D_{AS2} < D_{AS3}$) were inversely correlated with absorption coefficients ($\varepsilon_{365\ nm,\ AS1} > \varepsilon_{365\ nm,\ AS2} > \varepsilon_{365\ nm,\ AS3}$; $\varepsilon_{405\ nm,\ AS1} > \varepsilon_{405\ nm,\ AS2} > \varepsilon_{405\ nm,\ AS3}$). This was attributed to the fact that a smaller dihedral angle means a better coplanarity between the chalcone plane and the connected benzene plane, thereby enhancing the light-absorption [45]. With the smallest dihedral angle among four OXEs, AS1 exhibited the most favorable light absorption properties.

Steady-state photolysis experiments were performed to study the photochemical mechanism of chalcones and OXEs. As illustrated in Fig. 3c and Fig. S18b, both AS and BS exhibited significant photobleaching properties, with rapid intensity decreased at their maximum absorption peaks within 2 min under exposure to LED@365 nm. The photobleaching mechanism of chalcone has been extensively studied that the carbonyl in chalcone structure is destroyed under illumination, leading to the destruction of the entire conjugated structure [27,29,46]. Derived from chalcones, all four OXEs exhibited similar photolysis behavior to their respective chalcones (Fig. 3d and Figs. S18c-f). And they also displayed rapid photolysis rate in the visible-light region under LED@365 nm, which suggested a comparable photobleaching mechanism with chalcones. In this section, the outstanding light-absorption properties of chalcones and OXEs have been confirmed, indicating the effectiveness of our strategy to combine chalcone with diphenyl sulfide.

To gain insight into the excitation features of the chalcones and OXEs, energy level transition information was computed through time-dependent density functional theory (TD-DFT). The first ten singlet excitations and oscillator strengths of six compounds were depicted in Table S2 (Supporting information), and the calculated absorption peaks was corresponded with the measured UV–vis spectra, as illustrated in Figs. 4a and b, and Fig. S20 (Supporting information, right). For all six compounds, the S_0 (ground state) $\rightarrow S_1$ (lowest singlet excited state) excitations were negligible, exhibiting very weak oscillator strengths ($f < 0.01$). The theoretical predicted maximum wavelength (λ_{max}) for AS and BS on the low energy side

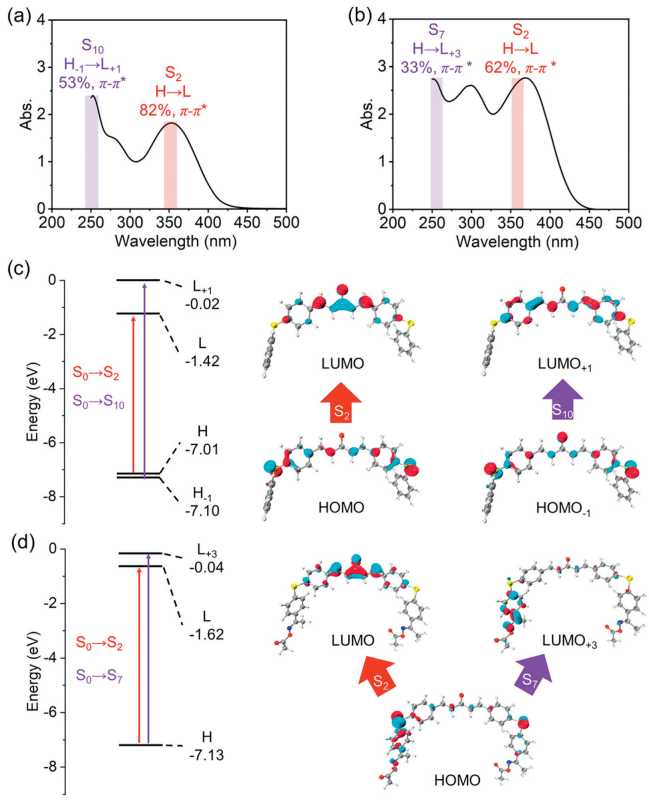

Fig. 4. UV–vis absorption spectra of (a) AS and (b) AS1, with the absorption peaks marked along with their corresponding transitions. Frontier molecular orbital diagrams with several main transitions of (c) AS and (d) AS1. The acronyms of HOMO and LUMO stand for highest occupied molecular orbital and lowest unoccupied molecular orbital, respectively.

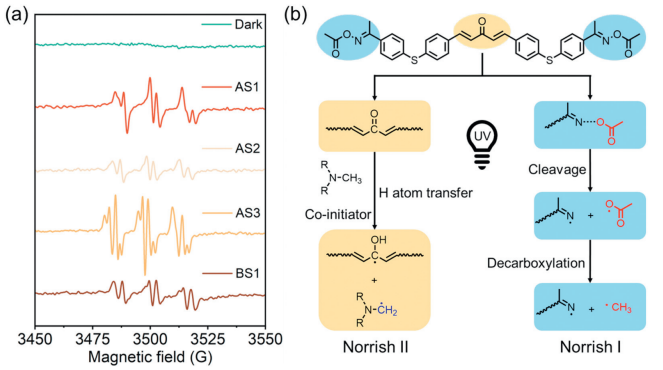

Fig. 5. (a) EPR spectra of the radicals captured by PBN in DMF under exposure to LED@365 nm. Light intensity is 100 mW/cm^2. (b) Proposed radical generation mechanism of AS1.

were 354 and 344 nm, respectively, corresponding to $S_0 \rightarrow S_2$ excitations with strong oscillator strengths (1.6779 and 1.6776, respectively). The OXEs displayed similar calculated λ_{max} to chalcones, with $\lambda_{max,\ AS1} = 352$ nm, $\lambda_{max,\ AS2} = 352$ nm, $\lambda_{max,\ AS3} = 352$ nm and $\lambda_{max,\ BS1} = 339$ nm. In addition to S_2 excitations, S_6 (AS3 and BS1) or S_7 (AS1 and AS2) excitations also exhibited relatively strong oscillator strength with absorption at about 260 nm, attributed to the absorption of the OXE moiety.

The frontier molecular orbitals of six compounds were computed and illustrated in Figs. 4c and d and Fig. S20 (left) to analyze the detailed mechanism of orbital transition progress. AS and AS1 were chosen as examples to elucidate the intrinsic relationship between chalcone moiety and OXE moiety. As shown in Table S1, the $\pi_{HOMO} \rightarrow \pi_{LUMO}$ transition of AS (82%) and AS1 (62%) constitute the primary type of their S_2 excitations, respectively. The $\pi_{HOMO} \rightarrow \pi_{LUMO}$ transition of AS (Fig. 4c) reveals significant electronic delocalization from the diphenyl sulfide moiety (primarily the sulfur atom) to the conjugate system of bis-chalcone moiety, indicating the effective enhancement on the conjugated system by the sulfur atom. Furthermore, as demonstrated in Fig. 4d, the $\pi_{HOMO} \rightarrow \pi_{LUMO}$ transition of AS1 is closely resembles that of AS, showing the significance of chalcone moiety in constructing the conjugate system and enhancing the light absorption property of OXE. This resemblance is also found in AS2, AS3 and BS1 (Fig. S20), further validating the effectiveness of the molecular construction strategy by combining chalcone and OXE. On the other hand, the $\pi_{HOMO} \rightarrow \pi_{LUMO+3}$ transition of AS1, corresponding to the S_7 excitation, reveals an obvious electronic delocalization over OXE moiety, leading to high reactivity of the N–O bond [39]. The results of theoretical simulations elucidate the effects of the conjugated structure composed of chalcone and diphenyl sulfide on orbital transitions and electron transfer, further illustrating the subtlety of the molecular design.

To analyze the type of free radicals generated by OXEs under illumination, electron spin resonance spin trapping (ESR-ST) experiments were conducted and the free radicals produced by four OXEs were trapped by PBN in DMF (Fig. 5a). The hyperfine coupling constants for the radical adduct generated by AS1 are $\alpha_N = 15.10$ G and $\alpha_H = 3.60$ G, which can be assigned to the methyl radical ($CH_3\cdot$) [47]. Similarly, the radical adducts generated by the other three OXEs were assigned and summarized in Table S3 (Supporting information), confirming the cleavage of N–O bond in OXE and the subsequent decarboxylation reaction under irradiation [22,38]. Taking AS1 as an example, the free radical generation mechanism of OXEs is illustrated in Fig. 5b. Firstly, a transition of AS1 occurred upon its excitation under irradiation, leading to the generation of free radicals through two different pathways. Regarding the chalcone moiety, a hydrogen atom abstraction reaction occurs between the carbonyl in chalcone moiety and amine-linked methyl/ethyl in the co-initiator, resulting in the generation of corresponding radicals (Norrish II) [27,29,46]. And for the OXE moiety, the cleavage of N–O bond is thermodynamically favorable due to its low bond energy, leading to the generation of carbonyl oxygen radical and nitrogen free radical with low initiation activity. Subsequently, the decarboxylation reaction of carbonyl oxygen radical occurs with the generation of carbon dioxide and the highly active methyl radical (Norrish I). The two coexistent mechanisms for free radical generation contributed to the rapid photopolymerization rate and curing integrity of OXEs. Moreover, the multiple initiating methods can expand the application potential of OXEs in complex environments.

The photoinitiating performance is the primary criteria for evaluating a PI. And monitoring the DBC of monomers under illumination using FTIR is a common method to evaluate photoinitiating performance. As shown in Figs. 6a and b, and Fig. S21 (Supporting information), three commonly used commercial monomers or oligomers were selected to assess the potential of four OXEs for application as PIs under LED@365 nm. Additionally, OXE-02 was tested under identical condition to serve as a control group. The DBC data are summarized in Table S4 (Supporting information). The results indicate that all four newly synthesized OXEs demonstrate outstanding photoinitiating properties in three monomers, indicating their effectiveness and versatility as PIs with LED as light source. Among them, the AS1 showed the most favorable photoinitiating performance compared to AS2 and AS3 (Fig. 6c), which could be attributed to their disparities in light-absorption and the generation of free radicals. Specifically, AS1 exhibited a higher absorption coefficient (365 nm) of 2.75, compared to AS2 (2.30) and AS3 (2.26), as shown in Table S1. Moreover, the methyl

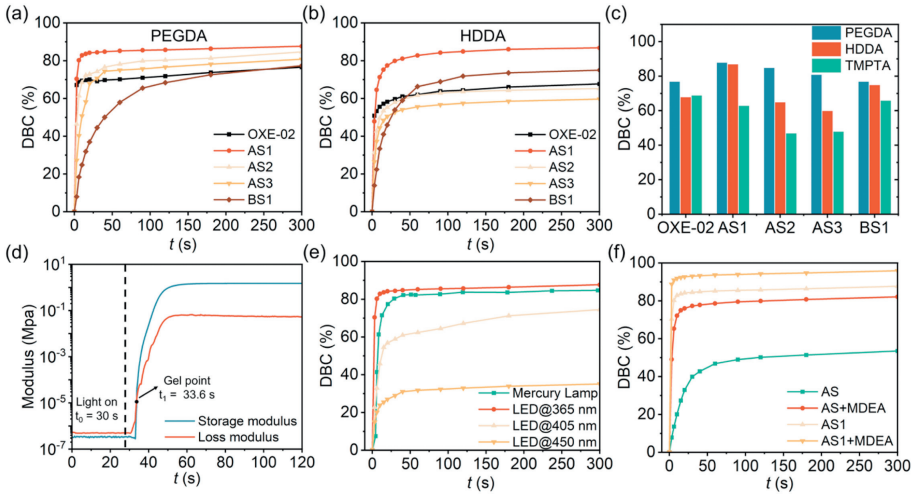

Fig. 6. Curves of (a) PEGDA and (b) HDDA polymerization initiated by four OXEs and OXE-02 under exposure to LED@365 nm. (c) Photoinitiation performance comparison of four OXEs in PEGDA, HDDA and TMPTA under LED@365 nm for 300 s. (d) Photorheological test of PEGDA with AS1. The intersection of the loss modulus and storage modulus curves is the gel point, and t_{gel} (s) = t_1 (s) −30. (e) AS1 in PEGDA under different light sources (Light intensity $I_{Mercury} = I_{365} = I_{405} = I_{450} = 100\ mW/cm^2$). (f) AS/AS1 with co-initiator MDEA in PEGDA under LED@365 nm. For all experiments above, the concentration of MDEA and PIs are 1.5×10^{-5} mol/g, and DBC represents the double bond conversion rate.

substituent ($-CH_3$) on ester exhibits higher reactivity in initiating polymerization compared to *n*-pentyl substituent [$-CH_2(CH_2)_3CH_3$] and benzene substituent ($-C_6H_5$) [22]. In addition, photorheological experiments also demonstrated the remarkable photoinitiating performance of AS1. As shown in Fig. 6d, the point of intersection (gel point) between the storage modulus curve and the loss modulus curve emerged at 3.6 s after the initiation of irradiation, indicating a notably rapid photoinitiating rate superior to that of AS2 (4.8 s), AS3 (10.5 s) and BS1 (no gel point observed) (Table S5 in Supporting information). Furthermore, AS1 exhibited clear superiority over OXE-02 in PEGDA and HDDA with the impressively rapid polymerization rate and high final DBC (FDBC, t = 300 s), indicating significant potential in the photocuring field. Despite achieving relatively high FDBC values, polymerizations initiated by BS1 displayed slower curing rate compared to other groups, with initial DBC (IDBC, t = 3 s) values of 8%, 14% and 24% for PEGDA, HDDA and TMPTA, respectively. Moreover, BS1 exhibited inadequate photoinitiating performance, as evidenced by the absence of a gel point observed in photorheological experiments after 60 s of irradiation. These results could be attributed to the distorted conformation of cyclohexanone-based bis-chalcone, which impedes electron delocalization and consequently delays excitation and photochemical reactions.

Considering the brilliant photoinitiation properties of AS1, further experiments were conducted to elucidate the polymerization process in detail. A concentration gradient experiment was carried out on AS1 to investigate the influence of dosage on photoinitiation performance. As illustrated in Fig. S22a (Supporting information), as the concentration increased from 0.05 wt% to 0.50 wt%, both the IDBC and FDBC showed a noticeable increase (IDBC from 16% to 39%; FDBC from 34% to 87%). However, this increase slowed down when the concentration was further raised from 0.50 wt% to 1.00 wt% (IDBC from 39% to 70%; FDBC from 87% to 88%. Apart from dosage, light intensity also exhibited a strong influence on photoinitiation ability. With the light intensity of LED@365 nm escalating from 10 mW/cm^2 to 100 mW/cm^2 (Fig. S22b in Supporting information), the IDBC showed noticeable growth (from 5% to 70%), while the change in FDBC was small (from 73% to 87%). In addition, the choice of light source exerts significant influence on photopolymerization, and thus the photoinitiation performance of AS1 under different light sources was characterized in Fig. 6e. According to the results, AS1 demonstrated suitability under exposure to mercury lamp, near-ultraviolet LED (365 nm) and visible-light (405 nm) LED with high FDBC of 85%, 88% and 74%, respectively. However, the FDBC under LED@450 nm remained modest (35%), attributed to the weak absorption of AS1 at 450 nm.

In the above experiments, the hydrogen abstraction reaction of the carbonyl in chalcone was restrained due to the absence of co-initiators, suggesting that free radicals were mainly generated by the OXE moiety. To assess the contribution of the chalcone moiety, co-initiator MDEA, along with AS/AS1, was employed to initiate the photopolymerization of PEGDA under LED@365 nm illumination (Fig. 6f). The carbonyl hydrogen abstraction process is highly dependent on the hydrogen donor (MDEA), which is the reason that the Type II free radical formation mechanism is ignored in AS group and AS1 group. Thus, the AS+MDEA group represents Type II free radical formation mechanism (carbonyl hydrogen abstraction), while the AS1 group represents Type I free radical formation mechanism (homolysis of oxime ester bond). According to the results, the AS1 group shows significantly higher DBC (IDBC = 70%; FDBC = 88%) compared to the AS+MDEA group (IDBC = 49%; FDBC = 82%). This result suggests that the Type I free radical formation mechanism plays a dominant role in photopolymerization. Moreover, the AS1+MDEA group combines both Type I and Type II free radical formation mechanisms, exhibiting the most outstanding photoinitiating abilities with the highest DBC values (IDBC = 89%; FDBC = 96%). The result suggests that the free radicals generated by N–O bond cleavage exhibit greater reactivity and thus play a predominant role in photopolymerization.

It is well-documented that chalcone exhibits significant photosensitivity and a favorable energy transfer relationship with iodonium salt and co-initiator [29-31,34]. Here, two three-component photoinitiation systems, AS/Iod/MDEA (0.1%/2%/2%, w/w/w), and AS1/Iod/MDEA (0.1%/2%/2%, w/w/w), were designed to explore the photosensitivity of AS and AS1 in free radical polymerization of PEGDA. As depicted in Fig. S23 (Supporting information), both two groups exhibited outstanding photoinitiation ability under LED@365 nm and LED@405 nm. Furthermore, the presence of AS/AS1 significantly enhanced the photoinitiating ability of Iod/MDEA two-component photoinitiating systems under LED@405 nm (IDBC from 18% to 67%/74%, FDBC from 62% to 84%/86%) (Table S6 in Supporting information). Unlike the re-

sults in Fig. 6f, AS/Iod/MDEA and AS1/Iod/MDEA groups exhibited similar photoinitiating abilities, which could be attributed to the low concentration of AS and AS1. Meanwhile, this similar photoinitiating performance suggests an energy interaction between the chalcone moiety and Iod. In summary, four OXEs exhibit exceptional photoinitiating abilities in free radical polymerization, clearly showing the enhancing effect of the OXE moiety on photoinitiating performance.

In summary, we successfully combined chalcone, diphenyl sulfides and OXE together, resulting in two novel bis-chalcones and four corresponding OXEs with outstanding light-absorption properties and photoinitiating performance. These compounds exhibited prominent absorption peaks at approximately 360 nm, which was attributed to the conjugated structure derived from bis-chalcone and two diphenyl sulfides evidenced by frontier molecular orbital simulations and excited state calculations. The four OXEs demonstrated outstanding free radical photoinitiating ability when exposed to LED@365 nm in acrylic monomers/oligomers. Particularly, AS1 achieved over 70% DBC within 3 s, which was superior to OXE-02. Moreover, high photoinitiating performance of AS1 (over 60% conversion) was attained at a relatively low concentration (1.5×10^{-6} mol/g). In addition to LED@365 nm, AS1 was also proved to be effective under visible LED, achieving over 70% conversion within 5 min. This study introduced an effective approach for constructing OXEs based on chalcone, offering insights for future molecular design endeavors in photopolymerization field.

Declaration of competing interest

The authors declare that they have no known competing financial interests or personal relationships that could have appeared to influence the work reported in this paper.

CRediT authorship contribution statement

Qian Wu: Writing – review & editing, Writing – original draft, Visualization, Validation, Software, Methodology, Investigation, Formal analysis, Data curation. **Mengda Xu:** Writing – review & editing, Validation, Supervision, Methodology, Investigation. **Tianjiao Ma:** Writing – review & editing, Validation, Funding acquisition, Formal analysis. **Shuzhen Yan:** Validation, Funding acquisition. **Jin Li:** Writing – review & editing, Validation, Supervision, Investigation, Funding acquisition. **Xuesong Jiang:** Writing – review & editing, Validation, Project administration, Methodology, Investigation, Funding acquisition, Formal analysis.

Acknowledgments

The authors thank National Nature Science Foundation of China (Nos. 52025032, 52103144 and 523B2026) for their financial support. This work was also supported by the Postdoctoral Fellowship Program of China Postdoctoral Science Foundation (No. GZC20231544).

Supplementary materials

Supplementary material associated with this article can be found, in the online version, at doi:10.1016/j.cclet.2024.110427.

References

[1] Y. Yagci, S. Jockusch, N.J. Turro, Macromolecules 43 (2010) 6245–6260.
[2] N. Corrigan, J. Yeow, P. Judzewitsch, et al., Angew. Chem. Int. Ed. 58 (2019) 5170–5189.
[3] K. Chung, Z.A. Page, J. Am. Chem. Soc. 145 (2023) 17912–17918.
[4] S. Shin, Y. Kwon, C. Hwang, et al., Adv. Mater. 36 (2024) 2311917.
[5] J. Zhang, P. Xiao, Polym. Chem. 9 (2018) 1530–1540.
[6] J.R. Tumbleston, D. Shirvanyants, N. Ermoshkin, et al., Science 347 (2015) 1349–1352.
[7] H. Li, B. Zhang, H. Ye, et al., Sci. Adv. 10 (2024) eadl4387.
[8] T.O. Machado, C.J. Stubbs, V. Chiaradia, et al., Nature 629 (2024) 1069–1074.
[9] T. Li, Z. Su, H. Xu, et al., Polym. Chem. 11 (2020) 1885–1893.
[10] X. Gao, J. Li, T. Li, et al., Adv. Funct. Mater. 31 (2021) 2106754.
[11] T. Ma, J. Bai, T. Li, et al., Proc. Natl. Acad. Sci. U. S. A. 118 (2021) e2114345118.
[12] S. Chen, K. Hu, S. Yan, et al., Sci. Bull. 67 (2022) 2186–2195.
[13] S. Yan, X. Deng, S. Chen, et al., Adv. Mater. 36 (2024) 2307445.
[14] W. Yuan, X. Deng, Z. Wang, et al., Adv. Mater. 36 (2024) 2400849.
[15] C. Dietlin, T.T. Trinh, S. Schweizer, et al., Molecules 25 (2020) 1671.
[16] N. Giacoletto, F. Dumur, Molecules 26 (2021) 3192.
[17] B. Bao, J. You, D. Li, et al., J. Photochem. Photobiol. C 429 (2022) 113938.
[18] F. Dumur, Eur. Polym. J. 169 (2022) 111120.
[19] F. Dumur, Eur. Polym. J. 159 (2021) 110734.
[20] W. Liao, J. Hou, H. Tang, et al., Org. Lett. 25 (2023) 6352–6356.
[21] X. Guo, Q. Zhou, X. Fan, et al., ACS Appl. Polym. Mater. 6 (2024) 5566–5575.
[22] S. Liu, N. Giacoletto, M. Schmitt, et al., Macromolecules 55 (2022) 2475–2485.
[23] C. Dworak, R. Liska, J. Polym. Sci. A: Polym. Chem. 48 (2010) 5865–5871.
[24] Z. Li, X. Zou, G. Zhu, et al., ACS Appl. Mater. Interfaces 10 (2018) 16113–16123.
[25] C. Zhuang, W. Zhang, C. Sheng, et al., Chem. Rev. 117 (2017) 7762–7810.
[26] S. Yen, J. Ni, Y. Chen, Eur. Polym. J. 187 (2023) 111885.
[27] T. Xue, Y. Li, L. Tang, et al., Dyes Pigm. 191 (2021) 109372.
[28] J. Li, M. Li, H. Song, et al., Chin. J. Polym. Sci. 11 (1993) 163–170.
[29] K. Sun, Y. Xu, F. Dumur, et al., Polym. Chem. 11 (2020) 2230–2242.
[30] Y. Xu, G. Noirbent, D. Brunel, et al., Eur. Polym. J. 132 (2020) 109737.
[31] Y. Xu, Z. Ding, H. Zhu, et al., J. Polym. Sci. 58 (2020) 3432–3445.
[32] J. Li, Q. Ding, K. Cao, et al., Eur. Polym. J. 196 (2023) 112291.
[33] H. Lu, J. Li, T. xue, et al., Eur. Polym. J. 190 (2023) 111992.
[34] F. Dumur, Eur. Polym. J. 195 (2023) 112193.
[35] S. Gong, X. Wu, Q. Liao, et al., Green Chem. 25 (2023) 2730–2744.
[36] X. Zhang, Z. Liu, D. Zhu, et al., Macromol. Chem. Phys. 224 (2023) 2300293.
[37] X. Wu, S. Gong, Z. Chen, et al., Dyes Pigm. 205 (2022) 110556.
[38] S. Chen, M. Jin, J. Malval, et al., Polym. Chem. 10 (2019) 6609–6621.
[39] R. Zhou, J. Malval, M. Jin, et al., Chem. Commun. 55 (2019) 6233–6236.
[40] W. Wang, M. Jin, H. Pan, D. Wan, Prog. Org. Coat. 151 (2021) 106019.
[41] J. Xu, G. Ma, K. Wang, et al., J. Appl. Polym. Sci. 123 (2012) 725–731.
[42] Q. Zou, Y. Zhao, N.S. Makarov, et al., Phys. Chem. Chem. Phys. 14 (2012) 11743–11752.
[43] D.E. Fast, A. Lauer, J.P. Menzel, et al., Macromolecules 50 (2017) 1815–1823.
[44] T.J.A. Wolf, D. Voll, C. Barner-Kowollik, A.N. Unterreiner, Macromolecules 45 (2012) 2257–2266.
[45] J. Xue, Y. Zhao, F. Wu, D.C. Fang, J. Phys. Chem. A 114 (2010) 5171–5179.
[46] J. Li, X. Zhang, S. Ali, et al., J. Photochem. Photobiol. C 384 (2019) 112037.
[47] E.G. Janzen, B.J. Blackburn, J. Am. Chem. Soc. 90 (1968) 5909–5910.